

# Super-Exponential Approximation of the Riemann-Liouville Fractional Integral via Shifted Gegenbauer Pseudospectral Methods

Kareem T. Elgindy<sup>a,b,\*</sup>

<sup>a</sup>Department of Mathematics and Sciences, College of Humanities and Sciences, Ajman University, P.O.Box: 346 Ajman, United Arab Emirates

<sup>b</sup>Nonlinear Dynamics Research Center (NDRC), Ajman University, P.O.Box: 346 Ajman, United Arab Emirates

## Abstract

This paper introduces a shifted Gegenbauer pseudospectral (SGPS) method for high-precision approximation of the left Riemann-Liouville fractional integral (RLFI). By using precomputable fractional-order shifted Gegenbauer integration matrices (FSGIMs), the method achieves super-exponential convergence for smooth functions, delivering near machine-precision accuracy with minimal computational cost. Tunable shifted Gegenbauer (SG) parameters enable flexible optimization across diverse problems, while rigorous error analysis confirms rapid error decay under optimal settings. Numerical experiments demonstrate that the SGPS method outperforms MATLAB's `integral`, MATHEMATICA's `NIntegrate`, and existing techniques by up to two orders of magnitude in accuracy, with superior efficiency for varying fractional orders  $0 < \alpha < 1$ . Its adaptability and precision make the SGPS method a transformative tool for fractional calculus, ideal for modeling complex systems with memory and non-local behavior.

**Keywords:** Riemann-Liouville fractional integral, Shifted Gegenbauer polynomials, Pseudospectral methods, Super-exponential convergence, Fractional-order integration matrix.

**MSC 2020 Classification:** 26A33, 41A10, 65D30.

## 1. Introduction

Fractional calculus provides a robust framework for modeling complex systems with memory and non-local behavior, with applications in viscoelasticity [1], anomalous diffusion [2], control theory [3], and beyond. Central to this field is the left RLFI, defined for  $\alpha \in (0, 1)$  and  $f \in L^2(\Omega_1)$  as indicated in Table 1. The singular kernel  $(t - \tau)^{\alpha-1}$  poses significant computational challenges, necessitating advanced numerical methods to achieve high accuracy without excessive computational cost.

Existing approaches to RLFI approximation include wavelet-based methods [4–9], polynomial and orthogonal function techniques [10–14], finite difference and quadrature schemes [15–18], and operational matrix methods [19–22]. Additional methods involve local meshless techniques [23], alternating direction implicit schemes [24], and radial basis functions [25]. While these methods have shown promise in specific contexts, they often struggle with trade-offs between accuracy, computational cost, and flexibility, particularly when adapting to diverse problem characteristics or varying fractional orders.

This study introduces the SGPS method, which overcomes these challenges through three key innovations: (i) *Parameter adaptability*, utilizing the tunable SG parameters  $\lambda$  (for interpolation) and  $\lambda_{n_q}$  (for quadrature approximation) to optimize performance across a wide range of problems; (ii) *Super-exponential convergence*, achieving rapid error decay for smooth functions,

often reaching near machine precision with modest node counts; and (iii) *Computational efficiency*, enabled by precomputable FSGIMs that minimize runtime costs. Numerical experiments demonstrate that the SGPS method significantly outperforms established tools like MATLAB's `integral` function and MATHEMATICA's `NIntegrate`, achieving up to two orders of magnitude higher accuracy in certain cases. It also surpasses prior methods, such as the trapezoidal approach of Dimitrov [26] and spline-based techniques of Ciesielski and Grodzki [27], in both precision and efficiency. Sensitivity analysis reveals that setting  $\lambda_q < \lambda$  accelerates convergence, while rigorous error bounds confirm super-exponential decay under optimal parameter choices. The FSGIM's invariance for fixed points and parameters enables precomputation, making the SGPS method ideal for problems requiring repeated fractional integrations with varying  $\alpha$ .

The paper is organized as follows: Section 2 presents the SGPS approximation framework. Section 3 analyzes computational complexity. Section 4 provides a detailed error analysis. Section 5 evaluates numerical performance. Finally, Appendix B includes supporting mathematical proofs.

## 2. Numerical Approximation of RLFI

This section presents the SGPS method adapted for approximating the RLFI. For foundational details on Gegenbauer and SG polynomials and their quadratures, see [28–31].

Let  $\alpha \in (0, 1)$ ,  $f \in L^2(\Omega_1)$ , and  $\{\hat{r}_{n,0:n}^\lambda\} = \mathbb{C}_r^\lambda$ . The SGPS

\*Corresponding author

Email address: k.elgindy@ajman.ac.ae (Kareem T. Elgindy)

**Table 1:** Table of Symbols and Their Meanings

| Symbol                                 | Meaning   | Symbol                               | Meaning  | Symbol                           | Meaning   |
|--|---|--------------------------------------|--|----------------------------------|---|
| $\forall$                              | for all   | $\forall_c$                          | for any  | $\forall_m$                      | for almost all  |
| $\forall_e$                            | for each  | $\forall_s$                          | for some   | $\forall_r$                      | for (a) relatively small  |
| $\forall_l$                            | for (a) relatively large  | $\ll$                                | much less than   | $\exists$                        | there exist(s)  |
| $\sim$                                 | asymptotically equivalent   | $\lesssim$                           | asymptotically less than   | $\#$                             | not sufficiently close to   |
| $\in$                                  | set of all complex-valued functions   | $\bar{\in}$                          | set of all real-valued functions   | $\mathbb{C}$                     | set of complex numbers  |
| $\mathbb{R}$                           | set of real numbers   | $\mathbb{R}_\neq$                    | set of nonzero real numbers  | $\mathbb{R}_\geq$                | set of non-negative real numbers  |
| $\mathbb{R}_{-1/2}$                    | $\{x \in \mathbb{R} : -1/2 < x < 0\}$   | $\mathbb{Z}$                         | set of integers  | $\mathbb{Z}^+$                   | set of positive integers  |
| $\mathbb{Z}_0^+$                       | set of non-negative integers  | $\mathbb{Z}_e^+$                     | set of positive even integers  | $i, j, k$                        | list of numbers from $i$ to $k$ with increment $j$  |
| $i, k$                                 | list of numbers from $i$ to $k$ with increment 1  | $y_{1:n}$ or $y_{i:n}$               | list of symbols $y_1, y_2, \dots, y_n$   | $\{y_{1:n}\}$                    | set of symbols $y_1, y_2, \dots, y_n$   |
| $\mathbb{I}_n$                         | $\{0 : n - 1\}$   | $\mathbb{I}_n^+$                     | $\mathbb{I}_n \cup \{n\}$  | $\mathbb{N}_n$                   | $\{1 : n\}$   |
| $\mathbb{N}_{m,n}$                     | $\{m : n\}$   | $\mathbb{G}_n^\lambda$               | set of Gegenbauer-Gauss (GG) zeros of the $(n + 1)$ st-degree Gegenbauer polynomial with index $\lambda > -1/2$      | $\mathbb{G}_n^\lambda$           | set of SGG points in the interval $[0, 1]$  |
| $\Omega_{a,b}$                         | closed interval $[a, b]$  | $\Omega^\circ$                       | interior of the set $\Omega$   | $\Omega_T$                       | specific interval $[0, T]$  |
| $\Omega_{x,T}$                         | Cartesian product $\Omega_x \times \Omega_T$  | $W$                                  | Lambert W function   | $\Gamma(\cdot)$                  | Gamma function  |
| $\Gamma(\cdot, \cdot)$                 | upper incomplete gamma function   | $\lceil \cdot \rceil$                | ceiling function   | $\mathbb{I}_{j \geq k}$          | indicator (characteristic) function $\begin{cases} 1 & \text{if } j \geq k \\ 0 & \text{otherwise} \end{cases}$ |
| $E_{\alpha,\beta}(z)$                  | two-parameter Mittag-Leffler function   | $(x)_m$                              | The generalized falling factorial $\frac{\Gamma(x+1)}{\Gamma(x-m+1)} \forall x \in \mathbb{C}, m \in \mathbb{Z}_0^+$ | $\text{supp}(f)$                 | support of function $f$   |
| $f^*$                                  | complex conjugate of $f$  | $f_c$                                | $f(t_c)$   | $f_{c,n}$                        | $f_c(t_n)$  |
| $I_{0:n}^\alpha h$                     | $\int_0^n h(t) dt$  | $I_{0:n}^\alpha h$                   | $\int_0^n h(t) dt$   | $I_{0:n}^\alpha h$               | $\int_0^n h(t) d(\cdot)$  |
| $I_{0:n}^\alpha h(t)$                  | $\int_0^n h(t) dt$  | $I_{0:n}^\alpha h(t)$                | $\int_0^n h(t) dt$   | $I_{0:n}^\alpha h$               | $\int_0^n h(t) dx$  |
| $\mathfrak{I}_t^\alpha f$              | The left RLFI defined by $\frac{1}{\Gamma(\alpha)} \int_0^t (t-\tau)^{\alpha-1} f(\tau) d\tau$                          | $\partial_x$                         | $d/dx$   | $\partial_x^\alpha$              | $d^\alpha/dx^\alpha$  |
| ${}^C D_t^\alpha f$                    | $\alpha$ th-order Caputo fractional derivative of $f$ at $x$  | $\text{Def}(\Omega)$                 | space of all functions defined on $\Omega$   | $C^k(\Omega)$                    | space of $k$ times continuously differentiable functions on $\Omega$  |
| $L^p(\Omega)$                          | Banach space of measurable functions $u \in \text{Def}(\Omega)$ with $\ u\ _{L^p} = (\int_\Omega  u ^p)^{1/p} < \infty$ | $L^\infty(\Omega)$                   | space of all essentially bounded measurable functions on $\Omega$  | $\ f\ _{L^\infty(\Omega)}$       | $L^\infty$ norm: $\sup_{x \in \Omega}  f(x)  = \inf\{M \geq 0 :  f(x)  \leq M \forall x \in \Omega\}$           |
| $\  \cdot \ _1$                        | $l_1$ -norm   | $\  \cdot \ _2$                      | Euclidean norm   | $\mathcal{S}^{(\alpha)}(\Omega)$ | Sobolev space of weakly differentiable functions with integrable weak derivatives up to order $\alpha$          |
| $t_N$                                  | $\{t_{0:N}, t_{1:N}, \dots, t_{N:N}\}^\top$   | $t_{0:N}$                            | $\{t_{0:N}, t_{1:N}, \dots, t_{N:N}\}^\top$  | $g^{(0:N)}$                      | $\{g, g', \dots, g^{(N)}\}^\top$  |
| $e^{0:N}$                              | $\{1, e, e^2, \dots, e^N\}$   | $t_{0:N}^\dagger$ or $\{t_{0:N,N}\}$ | $\{t_{0:N}, t_{1:N}, \dots, t_{N:N}\}$   | $h(y)$                           | vector with $i$ -th element $h(y_i)$  |
| $h(y)$ or $h_{1:n} \mathbf{h}^\dagger$ | $\{h_1(y), \dots, h_n(y)\}^\top$  | $y^\dagger$                          | vector of reciprocals of the elements of $y$   | $\mathbf{O}_n$                   | zero matrix of size $n$   |
| $f(n) = O(g(n))$                       | $\exists n_0, c > 0 : 0 \leq f(n) \leq cg(n) \forall n \geq n_0$  | $f(n) = o(g(n))$                     | $\lim_{n \rightarrow \infty} \frac{f(n)}{g(n)} = 0$  |                                  |   |

Remark: A vector is represented in print by a bold italicized symbol while a two-dimensional matrix is represented by a bold symbol, except for a row vector whose elements form a certain row of a matrix where we represent it in bold symbol.

interpolant of  $f$  is given by

$$I_n f(t) = f_{0:n}^\top \mathcal{L}_{0:n}^\lambda \mathbf{t} \mathbf{t}^\dagger, \quad (2.1)$$

where  $\mathcal{L}_k^\lambda(t)$  is defined as

$$\mathcal{L}_k^\lambda(t) = \hat{\omega}_k^\lambda \text{trp} \left( \hat{\lambda}_{0:n}^\lambda \right) \left( \hat{G}_{0:n}^\lambda \mathbf{t} \hat{t}_{n,k}^\lambda \right) \mathbf{t} \hat{G}_{0:n}^\lambda \mathbf{t} \mathbf{t}^\dagger, \quad \forall k \in \mathbb{J}_n^+, \quad (2.2)$$

with normalization factors and Christoffel numbers:

$$\hat{\lambda}_j^\lambda = \frac{\pi 2^{1-4\lambda} \Gamma(j+2\lambda)}{j! \Gamma^2(\lambda)(j+\lambda)},$$

$$\hat{\omega}_k^\lambda = 1 / \left[ \text{trp} \left( \hat{\lambda}_{0:n}^\lambda \right) \left( \hat{G}_{0:n}^\lambda \mathbf{t} \hat{t}_{n,k}^\lambda \right)_{(2)} \right],$$

$\forall j, k \in \mathbb{J}_n^+$ . In matrix form, we can write Eq. (2.2) as

$$\mathcal{L}_{0:n}^\lambda \mathbf{t} \mathbf{t}^\dagger = \text{diag} \left( \hat{\omega}_{0:n}^\lambda \right) \left( \hat{G}_{0:n}^\lambda \mathbf{t} \mathbf{I}_{n+1} \right) \odot \hat{G}_{0:n}^\lambda \mathbf{t} \hat{t}_{n,n}^\lambda \mathbf{t}^\dagger \hat{\lambda}_{0:n}^\lambda. \quad (2.3)$$

This allows us to approximate the RLFI as follows:

$$\mathfrak{I}_t^\alpha f \approx \mathfrak{I}_t^\alpha I_n f = f_{0:n}^\top \mathfrak{I}_t^\alpha \mathcal{L}_{0:n}^\lambda. \quad (2.4)$$

Using the transformation

$$\tau = t \left( 1 - y^{1/\alpha} \right), \quad (2.5)$$

Formula (2.4) becomes

$$\mathfrak{I}_t^\alpha f \approx \frac{t^\alpha}{\Gamma(\alpha+1)} f_{0:n}^\top \mathcal{I}_1^{(\alpha)} \mathcal{L}_{0:n}^\lambda \mathbf{t} \mathbf{t}^\dagger \left( 1 - y^{1/\alpha} \right). \quad (2.6)$$

Substituting Eq. (2.3) into Eq. (2.6):

$$\mathfrak{I}_t^\alpha f \approx \frac{t^\alpha}{\Gamma(\alpha+1)} \left[ \text{trp} \left( \hat{\lambda}_{0:n}^\lambda \right) \times \left( \mathcal{I}_1^{(\alpha)} \hat{G}_{0:n}^\lambda \mathbf{t} \mathbf{t}^\dagger \left( 1 - y^{1/\alpha} \right) \mathbf{I}_{n+1} \right) \odot \hat{G}_{0:n}^\lambda \mathbf{t} \hat{t}_{n,n}^\lambda \mathbf{t}^\dagger \text{diag} \left( \hat{\omega}_{0:n}^\lambda \right) \right] f_{0:n}. \quad (2.7)$$

For multiple points  $z_{0:M} \in \Omega_1 \forall_s M \in \mathbb{Z}_0^+$ , we extend Eq. (2.3):

$$\mathcal{L}_{0:n}^\lambda \mathbf{t} z_M \mathbf{t}^\dagger = \text{resh}_{n+1, M+1} \left[ \text{trp} \left( \hat{\lambda}_{0:n}^\lambda \right) \times \left( \hat{G}_{0:n}^\lambda \mathbf{t} z_M \otimes \mathbf{I}_{n+1} \right) \odot \hat{G}_{0:n}^\lambda \mathbf{t} \mathbf{I}_{M+1} \otimes \hat{t}_{n,n}^\lambda \right] \times \left( \mathbf{I}_{M+1} \otimes \text{diag} \left( \hat{\omega}_{0:n}^\lambda \right) \right).$$

Thus,

$$\mathfrak{I}_{z_M}^\alpha f \approx \frac{1}{\Gamma(\alpha+1)} \left[ z_M^{\circ \alpha} \odot \left( {}^E \hat{\mathbf{Q}}_n^\alpha f_{0:n} \right) \right], \quad (2.8)$$

where

$${}^E \hat{\mathbf{Q}}_n^\alpha = \text{resh}_{n+1, M+1}^\top \left[ \text{trp} \left( \hat{\lambda}_{0:n}^\lambda \right) \times \left( \mathcal{I}_1^{(\alpha)} \hat{G}_{0:n}^\lambda \mathbf{t} z_M \otimes \left( 1 - y^{1/\alpha} \right) \mathbf{I}_{n+1} \right) \odot \hat{G}_{0:n}^\lambda \mathbf{t} \mathbf{I}_{M+1} \otimes \hat{t}_{n,n}^\lambda \right] \times \left( \mathbf{I}_{M+1} \otimes \text{diag} \left( \hat{\omega}_{0:n}^\lambda \right) \right).$$

Alternatively,

$$\mathfrak{I}_{z_M}^\alpha f \approx {}^E \mathbf{Q}_n^\alpha f_{0:n},$$

where

$${}^E\mathbf{Q}_n^\alpha = \frac{1}{\Gamma(\alpha + 1)} \text{diag}(\mathbf{z}_M^{\circ\alpha}) {}^E\hat{\mathbf{Q}}_n^\alpha. \quad (2.9)$$

We term  ${}^E\mathbf{Q}_n^\alpha$  the “ $\alpha$ th-order FSGIM” for the RLFI and  ${}^E\hat{\mathbf{Q}}_n^\alpha$  the “ $\alpha$ th-order FSGIM Generator.” Eq. (2.8) is preferred for computational efficiency.

To compute  $\mathcal{I}_1^{(y)} \hat{G}_j^\lambda \{t(1 - y^{1/\alpha})\}$ , we can use the SGIRV  $\hat{\mathbf{P}} = \frac{1}{2}\mathbf{P}$  with SGG nodes  $\hat{\mathbf{t}}_{n_q}^{\lambda_q}$ :

$$\mathcal{I}_1^{(y)} \hat{G}_j^\lambda \{t(1 - y^{1/\alpha})\} \approx \hat{\mathbf{P}} \hat{G}_j^\lambda \left( t \left( 1 - \hat{\mathbf{t}}_{n_q}^{\lambda_q^{1/\alpha}} \right) \right), \quad \forall j \in \mathbb{J}_n^+, t \in \Omega_1, \quad (2.10)$$

cf. [29, Algorithm 6 or 7]. Formula (2.10) represents the  $(n_q, \lambda_q)$ -SGPS quadrature used for the numerical partial calculation of the RLFI. We denote the approximate  $\alpha$ th-order RLFI of a function at point  $t$ , computed using Eq. (2.10) in conjunction with either Eq. (2.8) or Eq. (2.9), by  ${}_{n_q, \lambda_q}^{n, \lambda, E} \mathfrak{S}_t^\alpha$ .

### 3. Computational Complexity

This section provides a computational complexity analysis of constructing the  $\alpha$ th-order FSGIM  ${}^E\mathbf{Q}_n^\alpha$  and its generator  ${}^E\hat{\mathbf{Q}}_n^\alpha$ . The analysis is based on the key matrix operations involved in the construction process, which we analyze individually in the following:

- The term  $\mathbf{z}_M^{\circ\alpha}$  involves raising each element of an  $(M + 1)$ -dimensional vector to the power  $\alpha$ . This operation requires  $O(M)$  operations.
- Constructing  ${}^E\mathbf{Q}_n^\alpha$  from  ${}^E\hat{\mathbf{Q}}_n^\alpha$  involves a diagonal scaling by  $\text{diag}(\mathbf{z}_M^{\circ\alpha})$ , which requires another  $O(Mn)$  operations.
- The matrix  ${}^E\hat{\mathbf{Q}}_n^\alpha$  is constructed using several matrix multiplications and elementwise operations. For each entry of  $\mathbf{z}_M$ , the dominant steps include:
  - The computation of  $\hat{G}_{0,n}^\lambda$  using the three-term recurrence relation requires  $O(n)$  operations per point. Since the polynomial evaluation is required for polynomials up to degree  $n$ , this requires  $O(n^2)$  operations.
  - The quadrature approximation involves evaluating a polynomial at transformed nodes. The cost of calculating  $\hat{\mathbf{P}}$  depends on the chosen methods for computing factorials and the Gamma function, which can be considered a constant overhead. The computation of  $\hat{\mathbf{t}}_{n_q}^{\lambda_q^{1/\alpha}}$  involves raising each element of the column vector  $\hat{\mathbf{t}}_{n_q}^{\lambda_q}$  to the power  $1/\alpha$ , which is linear in  $(n_q + 1)$ . The cost of the matrix-vector multiplication is also linear in  $n_q + 1$ . Therefore, the computational cost of this step is  $O(n_q)$  for each  $j \in \mathbb{J}_n^+$ . The overall cost, considering all polynomial functions involved, is  $O(nn_q)$ .
  - The Hadamard product introduces another  $O(n^2)$  operations.

- The evaluation of  $\text{trp}(\hat{\lambda}_{0,n}^{\lambda \circ})$  requires  $O(n)$  operations, and the product of  $\text{trp}(\hat{\lambda}_{0,n}^{\lambda \circ})$  by the result from the Hadamard product requires  $O(n^2)$  operations.
- The final diagonal scaling by  $\text{diag}(\hat{\omega}_{0,n}^\lambda)$  contributes  $O(n)$ .

Summing the dominant terms, the overall computational complexity of constructing  ${}^E\mathbf{Q}_n^\alpha$  is  $O(n(n + n_q))$  per entry of  $\mathbf{z}_M$ . Therefore, the total number of operations required to construct the matrix  ${}^E\mathbf{Q}_n^\alpha$  for all entries of  $\mathbf{z}_M$  is  $O(Mn(n + n_q))$ .

### 4. Error Analysis

The following theorem establishes the truncation error of the  $\alpha$ th-order SGPS quadrature associated with the  $\alpha$ th-order FSGIM  ${}^E\mathbf{Q}_n^\alpha$  in closed form.

**Theorem 4.1.** *Suppose that  $f \in C^{n+1}(\Omega_1)$  is approximated by the SGPS interpolant (2.1). Assume also that the integrals*

$$\mathcal{I}_1^{(y)} \hat{G}_{0,n}^\lambda \{t(1 - y^{1/\alpha})\},$$

*are computed exactly  $\forall_a t \in \Omega_1$ . Then  $\exists \xi = \xi(t) \in \Omega_1^\circ$  such that the truncation error,  ${}^\alpha \mathcal{T}_n^\lambda(t, \xi)$ , in the RLFI approximation (2.7) is given by*

$${}^\alpha \mathcal{T}_n^\lambda(t, \xi) = \frac{t^\alpha f^{(n+1)}(\xi)}{(n + 1)! \Gamma(\alpha + 1) \hat{K}_{n+1}^\lambda} \mathcal{I}_1^{(y)} \hat{G}_{n+1}^\lambda \{t(1 - y^{1/\alpha})\}. \quad (4.1)$$

*Proof.* The Lagrange interpolation error associated with the SGPS interpolation (2.1) is given by

$$f(t) = I_n f(t) + \frac{f^{(n+1)}(\xi)}{(n + 1)! \hat{K}_{n+1}^\lambda} \hat{G}_{n+1}^\lambda(t), \quad (4.2)$$

where  $\hat{K}_{n+1}^\lambda$  is the leading coefficient of the  $(n + 1)$ st-degree,  $\lambda$ -indexed SG polynomial. Applying the RLFI operator  $\mathfrak{S}_t^\alpha$  on both sides of Eq. (4.2) results in the truncation error

$${}^\alpha \mathcal{T}_n^\lambda(t, \xi) = \frac{f^{(n+1)}(\xi)}{(n + 1)! \hat{K}_{n+1}^\lambda} \mathfrak{S}_t^\alpha \hat{G}_{n+1}^\lambda. \quad (4.3)$$

The proof is accomplished from Eq. (4.3) by applying the change of variables (2.5) on the RLFI of  $\hat{G}_{n+1}^\lambda$ .  $\square$

The following theorem provides an upper bound for the truncation error (4.1).

**Theorem 4.2.** *Let  $\|f^{(n)}\|_{L^\infty(\Omega_1)} = \mathcal{A}_n$ , and suppose that the assumptions of Theorem 4.1 hold. Then the truncation error  ${}^\alpha \mathcal{T}_n^\lambda(t, \xi)$  satisfies the asymptotic bound*

$$|{}^\alpha \mathcal{T}_n^\lambda(t, \xi)| \lesssim \mathcal{A}_{n+1} \vartheta_{\alpha, \lambda} \left( \frac{e}{4} \right)^n n^{-\frac{3}{2} - n + \lambda} \Upsilon_{\sigma, \lambda}(n) \quad \forall_n n, \quad (4.4)$$

where

$$\Upsilon_{\sigma^\lambda}(n) = \begin{cases} 1, & \lambda \in \mathbb{R}_0^+, \\ \sigma^\lambda n^{-\lambda}, & \lambda \in \mathbb{R}_{-1/2}^-, \end{cases}$$

$\sigma^\lambda > 1$  is a constant dependent on  $\lambda$ , and

$$\vartheta_{\alpha,\lambda} = \frac{1}{4\pi} e^{\alpha+1} \alpha^{-\frac{1}{2}-\alpha} (1+2\lambda)^{-\frac{1}{2}-2\lambda} \left[ 1 + \frac{1}{1620(1+\lambda)^5} \right] \times \left[ \frac{(1+\lambda) \operatorname{csch}\left(\frac{1}{1+2\lambda}\right)}{1+2\lambda} \right]^{\frac{1}{2}+\lambda} \left[ \alpha \sinh\left(\frac{1}{\alpha}\right) \right]^{-\alpha/2} \left[ (1+\lambda) \sinh\left(\frac{1}{1+\lambda}\right) \right]^{\frac{1+\lambda}{2}}.$$

*Proof.* Observe first that  $t^\alpha \leq 1 \forall t \in \Omega_1$ . Notice also that

$$\frac{1}{(n+1)! \Gamma(\alpha+1) \hat{K}_{n+1}^\lambda} = \frac{2^{-2n-1} (2\lambda+1) \Gamma(\lambda+2) \Gamma(n+2\lambda+1)}{(\lambda+1) \Gamma(\alpha+1) \Gamma(2\lambda+2) \Gamma(n+2) \Gamma(n+\lambda+1)}, \quad (4.5)$$

by definition. The asymptotic inequality (4.4) results immediately from (4.1) after applying the sharp inequalities of the Gamma function [30, Ineq. (96)] on Eq. (4.5) and using [31, Lemma 5.1], which gives the uniform norm of Gegenbauer polynomials and their associated shifted forms.  $\square$

Theorem 4.2 manifests that the error bound is influenced by the smoothness of the function  $f$  (through its derivatives) and the specific values of  $\alpha$  and  $\lambda$  with super-exponentially decay rate as  $n \rightarrow \infty$ , which guarantees that the error becomes negligible even for moderate values of  $n$ . By looking at the bounding constant  $\vartheta_{\alpha,\lambda}$ , we notice that, while holding  $\lambda$  fixed, the factor  $\alpha^{-\frac{1}{2}-\alpha}$  decays exponentially as  $\alpha$  increases because  $\alpha^{-\alpha}$  dominates. For large  $\alpha$ ,  $\sinh(1/\alpha) \approx 1/\alpha$ , so the factor  $[\alpha \sinh(1/\alpha)]^{-\alpha/2}$  behaves like 1. Thus, it does not significantly affect the behavior as  $\alpha$  increases. The factor  $e^{\alpha+1}$  grows exponentially as  $\alpha$  increases. Combining these observations, the dominant behavior as  $\alpha$  increases is determined by the exponential growth of  $e^{\alpha+1}$  and the exponential decay of  $\alpha^{-\frac{1}{2}-\alpha}$ . The exponential decay dominates, so  $\vartheta_{\alpha,\lambda}$  decays as  $\alpha$  increases, leading to a tighter error bound and improved convergence rate. On the other hand, considering large  $\lambda$  values while holding  $\alpha$  fixed, the factor  $(1+2\lambda)^{-\frac{1}{2}-2\lambda}$  decays as  $\lambda$  increases. The factor  $1 + 1/(1620(1+\lambda)^5)$  approaches 1 as  $\lambda$  increases. For large  $\lambda$ ,  $\operatorname{csch}[1/(1+2\lambda)] \approx 1+2\lambda$ , so the factor  $\left[ \frac{(1+\lambda) \operatorname{csch}\left(\frac{1}{1+2\lambda}\right)}{1+2\lambda} \right]^{\frac{1}{2}+\lambda}$  behaves like  $(1+\lambda)^{\frac{1}{2}+\lambda}$ . This grows as  $\lambda$  increases. Finally, the factor  $\left[ (1+\lambda) \sinh\left(\frac{1}{1+\lambda}\right) \right]^{\frac{1+\lambda}{2}}$  behaves like 1 as  $\lambda$  increases. Thus, it does not significantly affect the behavior as  $\lambda$  increases. Combining these observations, the dominant behavior as  $\lambda$  increases is determined by the growth of  $(1+\lambda)^{\frac{1}{2}+\lambda}$  and the decay of  $(1+2\lambda)^{-\frac{1}{2}-2\lambda}$ . The decay of  $(1+2\lambda)^{-\frac{1}{2}-2\lambda}$  dominates, so  $\vartheta_{\alpha,\lambda}$  also decays as  $\lambda$  increases. It is noteworthy that  $\vartheta_{\alpha,\lambda}$  remains finite as  $\lambda \rightarrow -1/2$ , even though  $\lim_{\lambda \rightarrow -0.5^+} T_1(\lambda) = \infty$ , where  $T_1(\lambda) = (1+2\lambda)^{-\frac{1}{2}-2\lambda}$ . This divergence is offset by the behavior

of  $T_2(\lambda)$ :

$$T_2(\lambda) = \left[ \frac{(1+\lambda) \operatorname{csch}\left(\frac{1}{1+2\lambda}\right)}{1+2\lambda} \right]^{\frac{1}{2}+\lambda}.$$

Specifically, for  $\lambda \rightarrow -0.5^+$ , using the approximation  $\operatorname{csch}(x) \approx 2e^{-x}$  for large  $x$ :

$$T_2(\lambda) \approx \left[ \frac{(1+\lambda) \cdot 2e^{-\frac{1}{1+2\lambda}}}{1+2\lambda} \right]^{\frac{1}{2}+\lambda} \sim \left[ \frac{0.5 \cdot 2e^{-\frac{1}{0^+}}}{0^+} \right]^{0^+} \rightarrow 0.$$

Consequently,

$$\lim_{\lambda \rightarrow -0.5^+} T_1(\lambda) T_2(\lambda) = 0.$$

Hence,  $\vartheta_{\alpha,\lambda} \rightarrow 0$  as  $\lambda \rightarrow -1/2^+$ , driven by the product  $T_1(\lambda) T_2(\lambda) \rightarrow 0$ . For  $\lambda \in \mathbb{R}_{-1/2}^-$ , we notice that  $T_1$  is strictly concave with a maximum value at

$$\lambda^* = \frac{-e + e^{W(e/2)}}{2e} \approx -0.1351,$$

rounded to 4 significant digits; cf. Theorem Appendix B.1. Figure 2 shows further the plots of  $T_2(\lambda)$  and

$$T_3(\lambda) = \left[ (1+\lambda) \sinh\left(\frac{1}{1+\lambda}\right) \right]^{\frac{1+\lambda}{2}},$$

where  $T_2$  grows at a slow, quasi-linearly rates of change, while  $T_3$  decays at a comparable rate; thus, their product remains positive with a small bounded variation. This shows that, while holding  $\alpha$  fixed, the bounding constant  $\vartheta_{\alpha,\lambda}$  displays a unimodal behavior: it rises from 0 as  $\lambda$  increases from  $-1/2^+$ , attains a maximum at  $\lambda^* \approx -0.1351$ , and subsequently decays monotonically for  $\lambda > \lambda^*$ . Figure 1 highlights how  $\vartheta_{\alpha,\lambda}$  decays with increasing  $\alpha$  while exhibiting varying sensitivity to  $\lambda$ , with the  $\lambda = \lambda^*$  case (red curve) representing the parameter value that maximizes  $\vartheta_{\alpha,\lambda}$  for fixed  $\alpha$ .

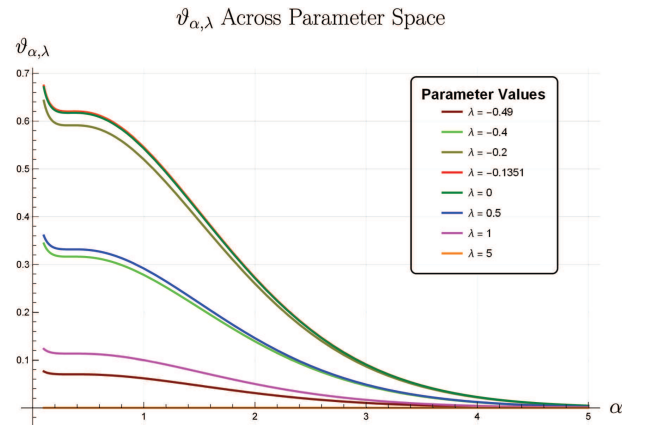


**Figure 1:** Behavior of the bounding constant  $\vartheta_{\alpha,\lambda}$  as  $\alpha$  varies from 0.1 to 5, shown for eight representative values of  $\lambda$  ( $-0.49$ ,  $-0.4$ ,  $-0.2$ ,  $-0.1351$ ,  $0$ ,  $0.5$ ,  $1$ , and  $5$ ). Each curve corresponds to a distinct  $\lambda$  value: dark red ( $\lambda = -0.49$ ), green ( $\lambda = -0.4$ ), olive ( $\lambda = -0.2$ ), bright red ( $\lambda = -0.1351$ ), dark green ( $\lambda = 0$ ), blue ( $\lambda = 0.5$ ), magenta ( $\lambda = 1$ ), and orange ( $\lambda = 5$ ).

It is important to note that the bounding constant  $\vartheta_{\alpha,\lambda}$  modulates the error bound without altering its super-exponential de-

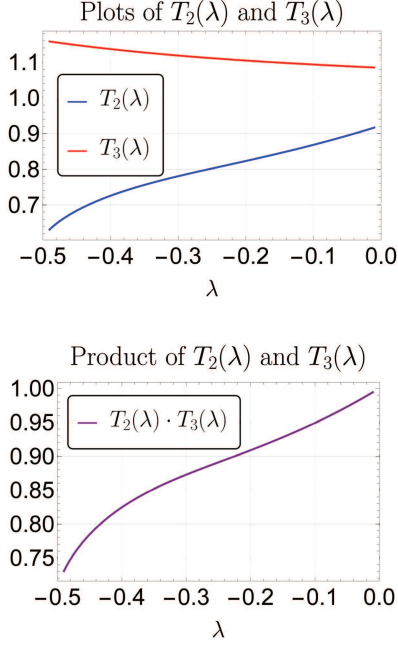


**Figure 2:** (Top) Comparison of the functions  $T_2$  (blue curve) and  $T_3$  (red curve) over the interval  $\mathbb{R}_{-1/2}^-$ . (Bottom) The product  $T_2 T_3$  (purple), showing the combined behavior of the two functions. All plots demonstrate the dependence on the parameter  $\lambda$  in the negative domain near zero.

can as  $n \rightarrow \infty$ . Near  $\lambda = -1/2$ ,  $\vartheta_{\alpha,\lambda} \rightarrow 0$ , which shrinks the truncation error bound, improving accuracy despite potential sensitivity in the SG polynomials. At  $\lambda = \lambda^*$ , the maximized  $\vartheta_{\alpha,\lambda}$  widens the bound, though it still vanishes as  $n \rightarrow \infty$ . Beyond  $\lambda = \lambda^*$ , the overall error bound decreases monotonically, despite a slower  $n$ -dependent decay for larger positive  $\lambda$ . The super-exponential term  $(\frac{e}{4n})^n$  ensures rapid convergence in all cases. The decreasing  $\vartheta_{\alpha,\lambda}$  after  $\lambda^*$ , combined with the fact that the truncation error bound (excluding  $\vartheta_{\alpha,\lambda}$ ) is smaller for  $-1/2 < \lambda \leq 0$  compared to its value for  $\lambda > 0$ , further suggests that  $\lambda = 0$  appears “optimal” in practice for minimizing the truncation error bound  $\forall n$  in a stable numerical scheme, given the SG polynomial instability near  $\lambda = -1/2$ . However, for relatively small or moderate values of  $n$ , other choices of  $\lambda$  may be optimal, as the derived error bounds are asymptotic and apply only as  $n \rightarrow \infty$ .

In what follows, we analyze the truncation error of the quadrature formula (2.10), and demonstrate how its results complement the preceding analysis.

**Theorem 4.3.** *Let  $j \in \mathbb{J}_n^+$ ,  $t \in \Omega_1$ , and assume that  $\hat{G}_j^\lambda(t(1-y^{1/\alpha}))$  is interpolated by the SG polynomials with respect to the variable  $y$  at the SGG nodes  $t_{n_q,0,n_q}^{\lambda_q}$ . Then  $\exists \eta = \eta(y) \in \Omega_1^c$  such that the truncation error,  $\mathfrak{T}_{j,n_q}^{\lambda_q}(\eta)$ , in the quadrature approximation (2.10) is given by*

$$\mathfrak{T}_{j,n_q}^{\lambda_q}(\eta) = \frac{(-1)^{n_q+1} \hat{\chi}_{j,n_q+1}^{\lambda_q}}{(n_q+1)! \hat{K}_{n_q+1}^{\lambda_q}} \left(\frac{t}{\alpha}\right)^{n_q+1} \eta^{\frac{(n_q+1)(1-\alpha)}{\alpha}} \times \hat{G}_{j-n_q-1}^{\lambda_q+n_q+1} \left(t(1-\eta^{\frac{1}{\alpha}})\right) \mathcal{I}_1^{(y)} \hat{G}_{n_q+1}^{\lambda_q} \cdot \mathbb{I}_{j \geq n_q+1}, \quad (4.6)$$

where  $\hat{\chi}_{n,m}^\lambda$  is defined by

$$\hat{\chi}_{n,m}^\lambda = \frac{n! \Gamma(\lambda+1/2) \Gamma(n+m+2\lambda)}{(n-m)! \Gamma(n+2\lambda) \Gamma(m+\lambda+1/2)} \quad \forall n \geq m, \quad (4.7)$$

cf. [32, Eq. (2.14)].

*Proof.* Let  $\hat{G}_j^{\lambda_q}$  denote the  $m$ th-derivative of  $\hat{G}_j^\lambda \forall j \in \mathbb{J}_n^+$ . [28, Theorem 4.1] tells us that

$$\mathfrak{T}_{j,n_q}^{\lambda_q}(\eta) = \frac{1}{(n_q+1)! \hat{K}_{n_q+1}^{\lambda_q}} \left[ \partial_y^{n_q+1} \hat{G}_j^\lambda \left( t(1-y^{\frac{1}{\alpha}}) \right) \right]_{y=\eta} \mathcal{I}_1^{(y)} \hat{G}_{n_q+1}^{\lambda_q} \quad (4.8)$$

Applying the Chain Rule on Eq. (4.8) gives

$$\mathfrak{T}_{j,n_q}^{\lambda_q}(\eta) = \frac{(-1)^{n_q+1}}{(n_q+1)! \hat{K}_{n_q+1}^{\lambda_q}} \left(\frac{t}{\alpha}\right)^{n_q+1} \eta^{\frac{(n_q+1)(1-\alpha)}{\alpha}} \times \hat{G}_j^{\lambda_q+n_q+1} \left( t(1-\eta^{\frac{1}{\alpha}}) \right) \mathcal{I}_1^{(y)} \hat{G}_{n_q+1}^{\lambda_q}. \quad (4.9)$$

The error bound (4.6) is accomplished by substituting [32, Eq. (2.13b)] into (4.9). The proof is complete by realizing that

$$\hat{G}_j^{\lambda_q+n_q+1} \left( t(1-\eta^{\frac{1}{\alpha}}) \right) = \partial_\tau^{n_q+1} \hat{G}_j^\lambda(\tau) \Big|_{\tau=t(1-\eta^{\frac{1}{\alpha}})} = 0,$$

$\forall j < n_q + 1$ .  $\square$

The next theorem provides an upper bound on the quadrature truncation error derived in Theorem 4.3.

**Theorem 4.4.** *Suppose that the assumptions of Theorem 4.3 hold true. Then the truncation error,  $\mathfrak{T}_{j,n_q}^{\lambda_q}(\eta)$ , in the quadrature approximation (2.10) vanishes  $\forall j < n_q + 1$ , and is bounded above by:*

$$\left| \mathfrak{T}_{j,n_q}^{\lambda_q}(\eta) \right| \lesssim \eta^{\frac{n_q(1-\alpha)}{\alpha}} \Upsilon_{\rho^{\lambda_q}}(n_q) \begin{cases} \mu_{\lambda,\lambda_q} n_q^{\lambda_q-\lambda} \left(\frac{2t}{\alpha}\right)^{n_q}, & j \sim n_q, \\ \frac{\gamma_{n_q}^{\lambda_q} j^{2(n_q+1)}}{\Theta_{\lambda_q} n_q^{3/2-\lambda_q}} \left(\frac{et}{2an_q}\right)^{n_q}, & j \gg n_q, \end{cases} \quad (4.10)$$

$\forall j \geq n_q + 1 \forall n_q$ , where  $\mu_{\lambda,\lambda_q} = \nu^\lambda / \Theta_{\lambda_q}$ ,  $\Theta_{\lambda_q}$  is as defined by (B.1),  $\nu^\lambda \in \mathbb{R}^+$  is a  $\lambda$ -dependent constant,  $\rho^{\lambda_q} > 1$  is a  $\lambda_q$ -dependent constant, and  $\gamma_{n_q}^{\lambda_q}$  is a constant dependent on  $n_q$  and  $\lambda$ .

*Proof.* Notice first that

$$\left| \hat{G}_{j-n_q-1}^{\lambda_q+n_q+1} \left( t(1-\eta^{\frac{1}{\alpha}}) \right) \right| \leq 1,$$

by [31, Lemma 5.1], since  $\lambda + n_q + 1 > 0$ . We now consider the following two cases.

**Case I ( $j \sim n_q$ ):** Lemmas Appendix B.1 and Appendix B.3 imply:

$$\frac{\hat{\chi}_{j,n_q+1}^\lambda}{(n_q+1)! \hat{K}_{n_q+1}^{\lambda_q}} \lesssim \frac{\nu^\lambda \left(\frac{4}{e}\right)^{n_q} n_q^{n_q+\frac{3}{2}-\lambda}}{\Theta_{\lambda_q} n_q^{3/2-\lambda_q} \left(\frac{2n_q}{e}\right)^{n_q}} = \mu_{\lambda,\lambda_q} 2^{n_q} n_q^{\lambda_q-\lambda}. \quad (4.11)$$

**Case II** ( $j \gg n_q$ ): Here  $\hat{\chi}_{j,n_q+1}^\lambda = O(j^{2(n_q+1)})$  by Lemma [Appendix B.1](#) and we have

$$\frac{\hat{\chi}_{j,n_q+1}^\lambda}{(n_q+1)! \hat{K}_{n_q+1}^{\lambda_q}} \lesssim \frac{\gamma_{n_q}^\lambda j^{2(n_q+1)}}{\Theta_{\lambda_q} n_q^{3/2-\lambda_q} \left(\frac{2n_q}{e}\right)^{n_q}}. \quad (4.12)$$

Formula (4.10) is obtained by substituting (4.11) and (4.12) into (4.6).  $\square$

When  $j \sim n_q$ , the dominant term in  $\sup \left| \hat{\mathfrak{T}}_{j,n_q}^{\lambda_q}(\eta) \right|$  becomes:

$$2^{n_q} n_q^{\lambda_q-\lambda} \cdot \left(\frac{t}{\alpha}\right)^{n_q} \eta^{\frac{n_q(1-\alpha)}{\alpha}} = \left(\frac{2t\eta^{\frac{1}{\alpha}-1}}{\alpha}\right)^{n_q} n_q^{\lambda_q-\lambda}.$$

Exponential decay occurs when:

$$\alpha > 2t\eta^{\frac{1}{\alpha}-1}. \quad (4.13)$$

On the other hand, the dominant term in the error bound  $\forall j \gg n_q$  is given by:

$$\begin{aligned} & \frac{\gamma_{n_q}^\lambda j^{2(n_q+1)}}{\Theta_{\lambda_q} n_q^{3/2-\lambda_q} \left(\frac{2n_q}{e}\right)^{n_q}} \cdot \left(\frac{t}{\alpha}\right)^{n_q} \eta^{\frac{n_q(1-\alpha)}{\alpha}} \\ &= \frac{\gamma_{n_q}^\lambda}{\Theta_{\lambda_q}} \left(\frac{etj^2\eta^{\frac{1}{\alpha}-1}}{2\alpha n_q}\right)^{n_q} j^{2n_q} n_q^{\lambda_q-3/2}. \end{aligned}$$

For convergence, we require:

$$\frac{etj^2\eta^{\frac{1}{\alpha}-1}}{2\alpha n_q} < 1.$$

Given  $j \gg n_q$ ,  $j^2/n_q \rightarrow \infty$ , and  $\frac{etj^2\eta^{\frac{1}{\alpha}-1}}{2\alpha n_q}$  typically diverges unless

$$\frac{t\eta^{\frac{1}{\alpha}-1}}{\alpha} \text{ is sufficiently small : } \left(\frac{etj^2\eta^{\frac{1}{\alpha}-1}}{2\alpha n_q}\right)^{n_q} j^{2n_q} n_q^{\lambda_q-3/2} \rightarrow 0. \quad (4.14)$$

The relative choice of  $\lambda$  and  $\lambda_q$  in either case controls the error bound's decay rate. In particular, choosing  $\lambda_q < \lambda$  ensures faster convergence rates when  $j \sim n_q$  due to presence of the polynomial factor  $n_q^{\lambda_q-\lambda}$ . For  $j \gg n_q$ , choosing  $\lambda_q < 3/2$  accelerates the convergence if Condition (4.14) holds.

The following theorem provides a rigorous asymptotic bound on the total truncation error for the RLFI approximation, combining both sources of error, namely, the interpolation and quadrature errors.

**Theorem 4.5** (Asymptotic Total Truncation Error Bound). *Suppose that  $f \in C^{n+1}(\Omega_1)$  is approximated by the SGPS interpolant (2.1), and the assumptions of Theorem 4.3 hold true. Then the total truncation error in the RLFI approximation of  $f$ , denoted by  ${}^\alpha \mathcal{E}_{n,n_q}^{\lambda,\lambda_q}(t,\xi,\eta)$ , arising from both the series truncation (2.1) and the quadrature approximation (2.10), is asymptotically bounded above by:*

$$\begin{aligned} & \left| {}^\alpha \mathcal{E}_{n,n_q}^{\lambda,\lambda_q}(t,\xi,\eta) \right| \lesssim \mathcal{A}_{n+1} \vartheta_{\alpha,\lambda} \left(\frac{e}{4}\right)^n n^{-\frac{3}{2}-n+\lambda} \Upsilon_{\sigma^\lambda}(n) \\ & + \frac{\mathcal{A}_0 \varpi^{\text{upp}} t^\alpha}{\lambda_{\max}^\lambda \Gamma(\alpha+1)} n(n-n_q) \eta^{\frac{n_q(1-\alpha)}{\alpha}} {}_2\Upsilon_{D^\lambda, \rho^{\lambda_q}}(n, n_q) \mathfrak{I}_{n \geq n_q+1} \times \end{aligned}$$

$$\begin{cases} \mu_{\lambda,\lambda_q} n_q^{\lambda_q-\lambda} \left(\frac{2t}{\alpha}\right)^{n_q}, & n \sim n_q, \\ \frac{\gamma_{n_q}^\lambda n^{2(n_q+1)}}{\Theta_{\lambda_q} n_q^{3/2-\lambda_q} \left(\frac{et}{2\alpha n_q}\right)^{n_q}}, & n \gg n_q, \end{cases}$$

$\forall n, n_q$ , where

$$\varpi^{\text{upp}} = \begin{cases} \varpi^{\text{upp},+}, & \forall \lambda \in \mathbb{R}_0^+, \\ \varpi^{\text{upp},-}, & \lambda \in \mathbb{R}_{-1/2}^-, \end{cases}$$

$$\frac{1}{\lambda_{\max}^\lambda} = \begin{cases} \frac{1}{\lambda_n^\lambda}, & \lambda \in \mathbb{R}_0^+, \\ \frac{1}{\lambda_{n_q+1}^\lambda}, & \lambda \in \mathbb{R}_{-1/2}^-, \end{cases}$$

$${}_2\Upsilon_{D^\lambda, \rho^{\lambda_q}}(n, n_q) = \begin{cases} 1, & \lambda \in \mathbb{R}_0^+, \quad \lambda_q \in \mathbb{R}_0^+, \\ D^\lambda n^{-\lambda}, & \lambda \in \mathbb{R}_{-1/2}^-, \quad \lambda_q \in \mathbb{R}_0^+, \\ \rho^{\lambda_q} n_q^{-\lambda_q}, & \lambda \in \mathbb{R}_0^+, \quad \lambda_q \in \mathbb{R}_{-1/2}^-, \\ D^\lambda \rho^{\lambda_q} n^{-\lambda} n_q^{-\lambda_q}, & \lambda \in \mathbb{R}_{-1/2}^-, \quad \lambda_q \in \mathbb{R}_{-1/2}^-, \end{cases}$$

with  $D^\lambda > 1$  being a  $\lambda$ -dependent constant, and  $\vartheta_{\alpha,\lambda}$ ,  $\Upsilon_{\sigma^\lambda}(n)$ ,  $\gamma_{n_q}^\lambda$ , and  $\Theta_{\lambda_q}$  are constants with the definitions and properties outlined in Theorems 4.2 and 4.4, and Lemmas [Appendix B.1](#) and [Appendix B.3](#), and  $\varpi^{\text{upp},\pm}$  are as defined by [[33, Formulas \(B.4\) and \(B.15\)](#)].

*Proof.* The total truncation error combines the interpolation error from Theorem 4.2 and the accumulated quadrature errors from Theorem 4.4 for  $j \in \mathbb{J}_n^+$ :

$$\begin{aligned} & {}^\alpha \mathcal{E}_{n,n_q}^{\lambda,\lambda_q}(t,\xi,\eta) = {}^\alpha \mathcal{T}_n^\lambda(t,\xi) \\ & + \frac{t^\alpha}{\Gamma(\alpha+1)} \sum_{k \in \mathbb{J}_n^+} \hat{\omega}_k^\lambda f_k \sum_{j \in \mathbb{J}_n^+} (\hat{\lambda}_j^\lambda)^{-1} \hat{\mathfrak{T}}_{j,n_q}^{\lambda_q}(\eta) \hat{G}_j^\lambda(\hat{x}_{n,k}^\lambda) \\ & = {}^\alpha \mathcal{T}_n^\lambda(t,\xi) + \frac{t^\alpha}{\Gamma(\alpha+1)} \sum_{k \in \mathbb{J}_n^+} \omega_k^\lambda f_k \sum_{j \in \mathbb{N}_{n_q+1,n}} (\lambda_j^\lambda)^{-1} \mathfrak{T}_{j,n_q}^{\lambda_q}(\eta) \hat{G}_j^\lambda(\hat{x}_{n,k}^\lambda). \end{aligned}$$

Using the bounds on Christoffel numbers  $\omega_k^\lambda$  and normalization factors  $\lambda_j^\lambda$  from [[33, Lemmas B.1 and B.2](#)], along with the uniform bound on Gegenbauer polynomials from [[31, Lemma 5.1](#)], we obtain:

$$\begin{aligned} & \left| {}^\alpha \mathcal{E}_{n,n_q}^{\lambda,\lambda_q}(t,\xi,\eta) \right| \lesssim \left| {}^\alpha \mathcal{T}_n^\lambda(t,\xi) \right| \\ & + \frac{\mathcal{A}_0 \varpi^{\text{upp}} t^\alpha}{\lambda_{\max}^\lambda \Gamma(\alpha+1)} (n+1)(n-n_q) \max_{j \in \mathbb{N}_{n_q+1,n}} \left| \mathfrak{T}_{j,n_q}^{\lambda_q}(\eta) \right| \Upsilon_{D^\lambda}(n). \end{aligned}$$

The proof is completed by applying Theorems 4.2 and 4.4 on Formula (4), noting that  $\max_{j \in \mathbb{N}_{n_q+1,n}} \left| \mathfrak{T}_{j,n_q}^{\lambda_q}(\eta) \right|$  occurs at  $j = n$ .

□

The total truncation error bound presented in Theorem 4.5 reveals several important insights about the convergence behavior of the RLFI approximation: (i) The total error consists of the interpolation error term  ${}^{\alpha}\mathcal{J}_n^{\lambda}(t, \xi)$  and the accumulated quadrature error term. The interpolation error term decays at a super-exponential rate  $\forall_r n$  due to the factor  $(\frac{e}{4n})^n$ . The quadrature error either vanishes when  $n_q \geq n$ , decays exponentially when  $n_q \sim n$  under Condition (4.13), or typically diverges when  $n \gg n_q$  unless Condition (4.14) is fulfilled. Therefore, the quadrature nodes should scale appropriately with the interpolation mesh size in practice. (ii) The interpolation error bound tightens as  $\alpha$  increases, due to the  $\vartheta_{\alpha, \lambda}$  factor's decay. The  $\lambda$  parameter shows a unimodal influence on the interpolation error, with potentially maximum error size at about  $\lambda^* \approx -0.1351$ . The  $\lambda_q$  parameter should generally be chosen smaller than  $\lambda$  to accelerate the convergence of the quadrature error when  $n_q \sim n$ . This analysis suggests that the proposed method achieves spectral convergence when the parameters are chosen appropriately. The quadrature precision should be selected to maintain balance between the two error components based on the desired accuracy and computational constraints.

## 5. Further Numerical Simulations

**Example 1.** To demonstrate the accuracy of the derived numerical approximation formulas, we consider the power function  $f(t) = t^N$ , where  $N \in \mathbb{Z}^+$ , as our first test case. The RLFI of  $f$  is given analytically by

$$\mathcal{I}_t^{\alpha} f(t) = \frac{N!}{\Gamma(N + \alpha + 1)} t^{N+\alpha}.$$

Figure 3 displays the logarithmic absolute errors of the RLFI approximations computed using the SGPS method, with fractional order  $\alpha = 0.5$  evaluated at  $t = 0.5$ . The figure consists of four subplots that investigate: (i) The effects of varying the parameters  $\lambda$ ,  $\lambda_{n_q}$ , and  $n_q$ , and (ii) a comparative analysis between the SGPS method and MATLAB's `integral` function with tolerance parameters set to `RelTol = AbsTol = 10-15`. Our numerical experiments reveal several key observations:

- Variation of  $\lambda$  while holding other parameters constant ( $\forall_r n, n_q$ ) shows negligible impact on the error. The error reaches near machine epsilon precision at  $n = 3$ , consistent with Theorems 4.1 and 4.3, which predict the collapse of both interpolation and quadrature errors when  $f^{(n+1)} \equiv 0$  and  $n_q > n$ .
- For  $n \geq 5$ , the total error reduces to pure quadrature error since  $f^{(n+1)} \equiv 0$  while  $n_q < n$ .
- Variation of  $\lambda_{n_q}$  significantly affects the error, with  $\lambda_{n_q} \leq \lambda$  generally yielding higher accuracy.
- Increasing either  $n$  or  $n_q$  while fixing the other parameter leads to exponential error reduction.

The SGPS method achieves near machine-precision accuracy with parameter values  $\lambda = \lambda_{n_q} = 0.5$  and  $n_q = 12$ , outperforming MATLAB's `integral` function by nearly two orders of magnitude. The method demonstrates remarkable stability, as evidenced by consistent error trends for  $\lambda_{n_q} \leq \lambda$ , with nearly exact approximations obtained for  $n_q \geq 12$  in optimal parameter ranges.

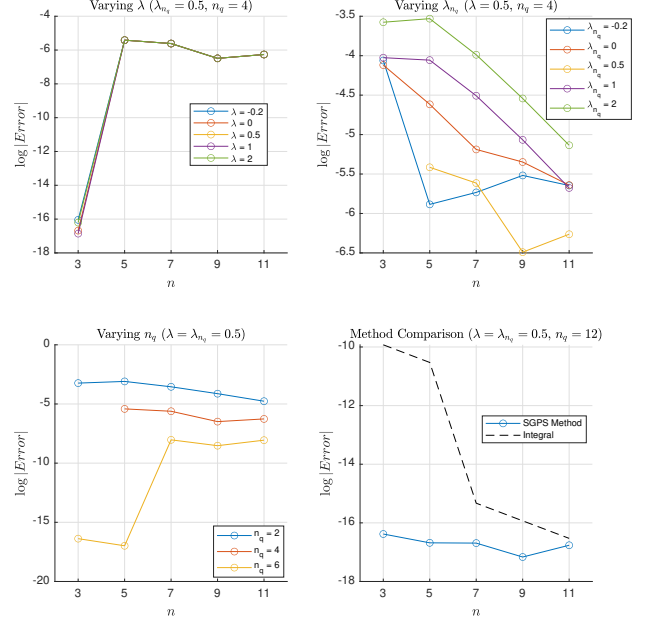


**Figure 3:** Logarithmic absolute errors of the RLFI approximations for the power function  $f$ , computed using the SGPS method. The fractional order is set to  $\alpha = 0.5$ , and approximations are evaluated at  $t = 0.5$ . Gegenbauer interpolant degrees match the function's degrees for  $n = 3 : 2 : 11$ . The figure presents errors under different conditions: *Top-left*: Varying  $\lambda$  with fixed  $\lambda_{n_q} = 0.5$  and  $n_q = 4$ . *Top-right*: Varying  $\lambda_{n_q}$  with fixed  $\lambda = 0.5$  and  $n_q = 4$ . *Bottom-left*: Varying  $n_q$  with  $\lambda = \lambda_{n_q} = 0.5$ . *Bottom-right*: Comparison between RLIM and MATLAB's `integral` function using  $n_q = 12$  and  $\lambda = \lambda_{n_q} = 0.5$ . "Error" refers to the difference between the true RLFI value and its approximation. Missing colored lines indicate zero error (approximation exact within numerical precision).

**Example 2.** Next, we evaluate the 0.5th-order RLFI of  $g(t) = e^{kt}$ , where  $k \in \mathbb{R} \setminus \{0\}$ , over  $\Omega_{0.5}$ . The analytical solution on  $\Omega_r$  is

$$\mathcal{I}_t^{\alpha} g(t) = \frac{t^{\alpha} e^{kt}}{\Gamma(\alpha + 1)} {}_1F_1(\alpha; \alpha + 1; -kt).$$

Figure 4 presents the logarithmic absolute errors of the SGPS approximations, with subplots analyzing: (i) the impact of  $\lambda$ ,  $\lambda_{n_q}$ ,  $n$ , and  $n_q$ , and (ii) a performance comparison against MATLAB's `integral` function (tolerances  $10^{-15}$ ). Some of the main findings include:

- Similar to **Example 1**, varying  $\lambda$  (with fixed small  $n, n_q$ ) has minimal effect on accuracy, whereas  $\lambda_{n_q} \leq \lambda$  consistently improves precision.
- Exponential error decay occurs when increasing either  $n$

or  $n_q$  while holding the other constant.

- Near machine-epsilon accuracy is achieved for  $\lambda = \lambda_{n_q} = 0.5$  and  $n_q = 12$ , with the SGPS method surpassing `integral` by two orders of magnitude.

The method's stability is further demonstrated by the uniform error trends for  $\lambda_{n_q} \leq \lambda$  and its rapid exponential convergence (see Figure 5), underscoring its suitability for high-precision fractional calculus, particularly in absence of closed-form solutions.

Notably, this test problem was previously studied in [26] and [27] on  $\Omega_2$ . The former employed an asymptotic expansion for trapezoidal RLFI approximation, while the latter used linear, quadratic, and three cubic spline variants, with all computations performed in 128-bit precision. The methods were tested for grid sizes  $N \in \{40, 80, 160, 320, 640\}$  (step sizes  $\Delta x \in \{0.05, 0.025, \dots, 0.003125\}$ ). At  $N = 640$ , Dimitrov's method achieved the smallest error of  $2.34 \times 10^{-13}$ , whereas Ciesielski and Grodzki [27] reported their smallest error of  $9.17 \times 10^{-13}$  using Cubic Spline Variant 1. With  $\lambda = \lambda_{n_q} = 0.5$  and  $n_q = 12$ , our method attains errors close to machine epsilon ( $\sim 10^{-16}$ ), surpassing both methods in [26] and [27] by several orders of magnitude, even with significantly fewer computational nodes.

**Example 3.** We evaluate the 0.5th-order Riemann-Liouville fractional integral (RLFI) of the function  $f(t) = 2t^3 + 8t$  over the interval  $\Omega_{0.5}$ . The analytical solution on  $\Omega_t$  is given by

$${}_0I_t^{0.5} f(t) = \frac{192t^{7/2} + 1120t^{3/2}}{105\sqrt{\pi}},$$

which serves as the reference for numerical comparison. Table 2 presents a comprehensive comparison of numerical results obtained using three distinct approaches: (i) The proposed SGPS method, (ii) MATLAB's high-precision `integral` function, and (iii) MATHEMATICA's `NIntegrate` function. This test case has been previously investigated by [34] on the interval  $\Omega_2$ . Their approach employed an  $n$ -point composite fractional formula derived from a three-point central fractional difference scheme, incorporating generalized Taylor's theorem and fundamental properties of fractional calculus. Notably, their implementation with  $n = 10$  subintervals achieved a relative error of approximately  $-6.87 \times 10^{-3}$ , which is significantly higher than the errors produced by the current method.

## 6. Conclusion

This study presents the SGPS method, a powerful approach for approximating the left RLFI. By using precomputable FS-GIMs, the method achieves super-exponential convergence for smooth functions, delivering near machine-precision accuracy with minimal computational effort. The tunable Gegenbauer parameters  $\lambda$  and  $\lambda_{n_q}$  enable tailored optimization, with sensitivity analysis showing that  $\lambda_{n_q} < \lambda$  accelerates convergence. Rigorous error bounds confirm rapid error decay, ensuring robust performance across diverse problems. Numerical results highlight the SGPS method's superiority, surpassing MATLAB's

**Table 2:** Comparison of the exact 0.5th-order RLFI of  $f(t) = 2t^3 + 8t$  over the interval  $[0, 0.5]$ , the SGPS method, MATLAB's `integral` function, and MATHEMATICA's `NIntegrate` function approximations. The table also includes the CPU times for computing the SGPS method and MATLAB's `integral` function. All relative error approximations are rounded to 16 significant digits. The CPU times were computed in seconds (s).

| Quantity  | Value              | Relative Error                      | CPU time    |
|---|--------------------|-------------------------------------|-------------|
| Exact Value   | 2.218878969089873  | —                                   | —           |
| SGPS Method Approximation<br>( $\lambda = \lambda_q = 0.5, n = 3, n_q = 4$ )  | 2.218878969089874  | $2.001412497195449 \times 10^{-16}$ | 0.003125 s  |
| MATLAB's <code>integral</code> Function Approximation<br>( $\text{RelTol} = \text{AbsTol} = 10^{-15}$ )               | 2.218878973119478  | $1.816054080462689 \times 10^{-9}$  | 0.015625 s  |
| MATHEMATICA's <code>NIntegrate</code> Function Approximation<br>( $\text{PrecisionGoal} = \text{AccuracyGoal} = 15$ ) | 2.2188789399346960 | $1.3139598073477670 \times 10^{-8}$ | 0.0098979 s |

`integral`, MATHEMATICA's `NIntegrate`, and prior techniques like trapezoidal [26] and spline-based methods [27] by up to several orders of magnitude in accuracy, while maintaining lower computational costs. The FSGIM's invariance for fixed points improves efficiency, making the method ideal for repeated fractional integrations with varying  $\alpha \in (0, 1)$ . These qualities establish the SGPS method as a versatile tool for fractional calculus, with significant potential to advance modeling of complex systems exhibiting memory and non-local behavior, and to inspire further innovations in computational mathematics.

## Declarations

### Competing Interests

The author declares there is no conflict of interests.

### Availability of Supporting Data

The author declares that the data supporting the findings of this study are available within the article.

### Ethical Approval and Consent to Participate and Publish

Not Applicable.

### Human and Animal Ethics

Not Applicable.

### Consent for Publication

Not Applicable.

### Funding

The author received no financial support for the research, authorship, and/or publication of this article.

### Authors' Contributions

The author confirms sole responsibility for the following: study conception and design, data collection, analysis and interpretation of results, and manuscript preparation.

## Appendix A. List of Acronyms

Table A.3: List of Acronyms

| Acronym | Meaning  |
|---------|--|
| FSGIM   | Fractional-order shifted Gegenbauer integration matrix |
| RLFI    | Riemann–Liouville fractional integral                  |
| SGIRV   | Shifted Gegenbauer integration row vector              |
| SGPS    | Shifted Gegenbauer pseudospectral                      |
| SG      | Shifted Gegenbauer                                     |
| SGG     | Shifted Gegenbauer-Gauss                               |

## Appendix B. MATHEMATICAL Theorems and Proofs

**Theorem Appendix B.1.** *The function  $T_1(\lambda) = (1 + 2\lambda)^{-1/2-2\lambda}$  is strictly concave over the interval  $-0.5 < \lambda < 0$ , and attains its maximum value at*

$$\lambda^* = \frac{-e + e^{W(e/2)}}{2e} \approx -0.1351,$$

rounded to 4 significant digits.

*Proof.* Notice that  $\ln T_1(\lambda) = (-1/2 - 2\lambda) \ln(1 + 2\lambda)$ . Thus,

$$\begin{aligned} \frac{d}{d\lambda} \ln T_1(\lambda) &= -2 \ln(1 + 2\lambda) - \frac{1 + 4\lambda}{1 + 2\lambda}, \\ \frac{d^2}{d\lambda^2} \ln T_1(\lambda) &= \frac{-6 - 8\lambda}{(1 + 2\lambda)^2}. \end{aligned}$$

For  $\lambda \in \mathbb{R}_{-1/2}^-$ ,  $(1 + 2\lambda)^2 > 0$ , and  $-6 - 8\lambda$  is linear and decreasing in  $\lambda$ . Thus,  $\frac{d^2}{d\lambda^2} \ln T_1(\lambda) < 0$  for all  $\lambda \in (-0.5, 0)$ . Since the logarithmic second derivative is negative,  $\ln T_1(\lambda)$  is strictly concave on  $(-0.5, 0)$ . Since the logarithm is a strictly increasing function and  $\ln T_1(\lambda)$  is strictly concave, then  $T_1(\lambda)$  itself is also strictly concave on the interval  $(-0.5, 0)$ . This proves the first part of the theorem. Now, to prove that  $T_1$  attains its maximum at  $\lambda^*$ , we set the logarithmic derivative equal to zero:

$$-2 \ln(1 + 2\lambda) - \frac{1 + 4\lambda}{1 + 2\lambda} = 0.$$

Let  $x = 1 + 2\lambda$ :

$$-2 \ln x - \frac{2x - 1}{x} = 0 \implies 2x \ln x + 2x - 1 = 0.$$

Let  $x = e^u$ :  $2ue^u + 2e^u - 1 = 0 \implies e^{u+1}(u+1) = \frac{e}{2}$ . The solution of this the transcendental equation is  $u = W(\frac{e}{2}) - 1$ . Thus,  $x = e^{W(e/2)}/e = 1 + 2\lambda$ , from which the maximum point  $\lambda = \lambda^*$  is determined. This completes the proof of the theorem.  $\square$

Figure B.6 shows a sketch of  $T_1$  on the interval  $\mathbb{R}_{-1/2}^-$ .

The following lemma establishes the asymptotic equivalence of  $(n_q + 1)! \hat{K}_{n_q+1}^{\lambda_q} \forall_{rl} n_q$ .

**Lemma Appendix B.1.** *Let  $\lambda_q > -\frac{1}{2}$  and consider the leading coefficient of the  $(n_q + 1)$ st-degree,  $\lambda_q$ -indexed SG polynomial defined by*

$$\hat{K}_{n_q}^{\lambda_q} = \frac{2^{n_q-1} \Gamma(2\lambda_q + 1) \Gamma(n_q + \lambda_q)}{\Gamma(\lambda_q + 1) \Gamma(n_q + 2\lambda_q)};$$

cf. [31, see p.g. 103]. Then,

$$(n_q + 1)! \hat{K}_{n_q+1}^{\lambda_q} \sim \Theta_{\lambda_q} n_q^{3/2-\lambda_q} \left(\frac{2n_q}{e}\right)^{n_q} \forall_{rl} n_q,$$

where

$$\Theta_{\lambda_q} = \frac{\sqrt{2\pi} \Gamma(2\lambda_q + 1)}{\Gamma(\lambda_q + 1)}. \quad (\text{B.1})$$

*Proof.* We begin by expressing  $\hat{K}_{n_q+1}^{\lambda_q}$  explicitly:

$$\hat{K}_{n_q+1}^{\lambda_q} = \frac{2^{n_q} \Gamma(2\lambda_q + 1) \Gamma(n_q + \lambda_q + 1)}{\Gamma(\lambda_q + 1) \Gamma(n_q + 2\lambda_q + 1)}.$$

Since

$$(n + 1)! \hat{K}_{n+1}^{\lambda_q} = O\left(n_q^{3/2-\lambda_q} \left(\frac{2n_q}{e}\right)^{n_q}\right), \quad \text{as } n_q \rightarrow \infty,$$

$\forall_a \lambda_q > -1/2$  by [35, Lemma 2.2] and [28, Lemma 4.2]. Then,

$$\frac{(n_q + 1)! \hat{K}_{n_q+1}^{\lambda_q}}{n_q^{3/2-\lambda_q} \left(\frac{2n_q}{e}\right)^{n_q}} = \frac{(n_q + 1)! e^{n_q} \Gamma(2\lambda_q + 1) \Gamma(n_q + \lambda_q + 1)}{\Gamma(\lambda_q + 1) \Gamma(n_q + 2\lambda_q + 1) n_q^{n_q - \lambda_q + 3/2}}.$$

Stirling's approximations to the factorial and gamma functions  $\forall_{rl} n_q$  give

$$\begin{aligned} (n_q + 1)! &\approx \sqrt{2\pi} n_q^{n_q+3/2} e^{-n_q}, \\ \Gamma(n_q + \lambda_q + 1) &\approx \sqrt{2\pi} n_q^{n_q + \lambda_q + 1/2} e^{-n_q}, \\ \Gamma(n_q + 2\lambda_q + 1) &\approx \sqrt{2\pi} n_q^{n_q + 2\lambda_q + 1/2} e^{-n_q}. \end{aligned}$$

Therefore,

$$\frac{(n_q + 1)! \Gamma(n_q + \lambda_q + 1)}{\Gamma(n_q + 2\lambda_q + 1)} = \sqrt{2\pi} n_q^{n_q - \lambda_q + 3/2} e^{-n_q}.$$

Multiplying by the remaining terms:

$$\frac{\Gamma(2\lambda_q + 1) e^{n_q}}{\Gamma(\lambda_q + 1) n_q^{n_q - \lambda_q + 3/2}} \cdot \sqrt{2\pi} n_q^{n_q - \lambda_q + 3/2} e^{-n_q} = \Theta_{\lambda_q}.$$

This shows that

$$\frac{(n + 1)! \hat{K}_{n+1}^{\lambda_q}}{n_q^{3/2-\lambda_q} \left(\frac{2n_q}{e}\right)^{n_q}} \sim \Theta_{\lambda_q} \forall_{rl} n_q,$$

which completes the proof.  $\square$

The next lemma is needed for the proof of the following lemma.

**Lemma Appendix B.2** (Falling Factorial Approximation). *Let  $n = m + k : k = o(m) \forall_r m \in \mathbb{Z}^+$ . Then the falling factorial satisfies:*

$$(n)_m = m^m \left(\frac{m}{k}\right)^{k+1/2} e^{k-m-\frac{1}{4k}-\frac{k^2}{2m}} \exp\left(O\left(\max\left(\frac{k^3}{m^2}, \frac{1}{k}\right)\right)\right).$$

*Proof.* Express the falling factorial as

$$(n)_m = \prod_{i=0}^{m-1} (m+k-i) = \prod_{j=1}^m (k+j).$$

Take logarithms to convert the product into a sum:

$$\ln(n)_m = \sum_{j=1}^m \ln(k+j).$$

Since  $m$  is large, we can approximate the sum by using the midpoint rule of integrals:

$$\begin{aligned} \sum_{j=1}^m \ln(k+j) &\approx \int_{1/2}^{m+1/2} \ln(k+x) dx \\ &= (k+m+\frac{1}{2}) \ln(k+m+\frac{1}{2}) - (k+\frac{1}{2}) \ln(k+\frac{1}{2}) - m. \end{aligned}$$

For  $k = o(m)$  and large  $m$ , Taylor series expansions produce:

$$\begin{aligned} (k+m+\frac{1}{2}) \ln(k+m+\frac{1}{2}) &= (k+m+\frac{1}{2}) \ln\left(m\left(1+\frac{k+\frac{1}{2}}{m}\right)\right) \\ &\approx m \ln m + m \left[ \frac{k+\frac{1}{2}}{m} - \frac{1}{2} \left(\frac{k+\frac{1}{2}}{m}\right)^2 + O\left(\left(\frac{k+\frac{1}{2}}{m}\right)^3\right) \right] \\ &= m \ln m + k + \frac{1}{2} - \frac{k^2}{2m} + O\left(\frac{k^3}{m^2}\right) + O\left(\frac{1}{m}\right), \end{aligned}$$

and

$$\begin{aligned} (k+\frac{1}{2}) \ln(k+\frac{1}{2}) &= (k+\frac{1}{2}) \left[ \ln k + \ln\left(1+\frac{1}{2k}\right) \right] \\ &= \frac{1}{2} + \frac{1}{4k} + (k+\frac{1}{2}) \ln k + O\left(\frac{1}{k}\right). \end{aligned}$$

Substituting these approximations back yields:

$$\begin{aligned} \ln(n)_m &\approx m \ln m - k \ln k + k - \frac{1}{2} \ln k - \frac{1}{4k} - m - \frac{k^2}{2m} \\ &\quad + O\left(\frac{k^3}{m^2}\right) + O\left(\frac{1}{k}\right). \end{aligned}$$

Exponentiating gives:

$$\begin{aligned} (n)_m &\approx m^m k^{-k} e^{k-m} k^{-1/2} e^{-1/(4k)} \exp\left(-\frac{k^2}{2m} + O\left(\frac{k^3}{m^2}\right) + O\left(\frac{1}{k}\right)\right) \\ &= m^{m-k} \left(\frac{m}{k}\right)^k e^{k-m} \sqrt{\frac{m}{k}} \frac{1}{\sqrt{m}} e^{-1/(4k)} \exp\left(-\frac{k^2}{2m} + O\left(\frac{k^3}{m^2}\right) + O\left(\frac{1}{k}\right)\right) \\ &= m^m \left(\frac{m}{k}\right)^{k+1/2} e^{k-m-\frac{1}{4k}-\frac{k^2}{2m}} \exp\left(O\left(\max\left(\frac{k^3}{m^2}, \frac{1}{k}\right)\right)\right). \end{aligned}$$

□

The next lemma gives the asymptotic upper bound on the

growth rate of the parametric scalar  $\hat{\chi}_{n,m}^\lambda$ .

**Lemma Appendix B.3.** *Let  $\lambda > -1/2$  and  $m \in \mathbb{Z}^+ : m \gg \lambda$ . Then*

$$\hat{\chi}_{n,m}^\lambda = \begin{cases} O\left(\left(\frac{4}{e}\right)^m m^{m+\frac{1}{2}-\lambda}\right) & \text{if } n \sim m, \\ O(n^{2m}) & \forall_r n \gg m. \end{cases}$$

*Proof.* Let  $n \sim m$ . Then  $n = m + k : k = o(m)$ , and we can write

$$(n)_m \approx m^{m+1/2} e^{-m},$$

by Lemma Appendix B.2. Substituting this approximation and the sharp inequalities of the Gamma function [30, Ineq. (96)] into Eq. (4.7) give:

$$\begin{aligned} \chi(n, m, \lambda) &\lesssim \hat{\ell}_\lambda m^{m+1/2} e^{-m} \cdot m^{-m-\lambda} n^{-n-2\lambda+\frac{1}{2}} (m+n)^{m+n+2\lambda-\frac{1}{2}} \\ &\sim \ell_\lambda \left(\frac{4}{e}\right)^m m^{m+\frac{1}{2}-\lambda}, \end{aligned}$$

where  $\ell_\lambda = \frac{4^\lambda}{\sqrt{2}} \hat{\ell}_\lambda$ , and  $\hat{\ell}_\lambda \in \mathbb{R}^+$  is a  $\lambda$ -dependent constant. Now, consider the case when  $n \gg m$ . Applying Stirling's approximation of factorials and the same sharp inequalities of the Gamma function on the parametric scalar  $\hat{\chi}_{n,m}^\lambda$  give:

$$\begin{aligned} \hat{\chi}_{n,m}^\lambda &\gtrsim h_m^\lambda n^{\frac{1}{2}+n} (n-m)^{\frac{1}{2}(-1+3m-3n)} (n+2\lambda-1)^{\frac{1}{2}-n-2\lambda} \times \\ &\quad (n+m+2\lambda-1)^{n+m+2\lambda-\frac{1}{2}} \sinh^{\frac{m-n}{2}} \left(\frac{1}{n-m}\right) \times \\ &\quad \left[ (n+2\lambda-1) \sinh\left(\frac{1}{n+2\lambda-1}\right) \right]^{\frac{1}{2}(1-n-2\lambda)} \times \\ &\quad \left[ (n+m+2\lambda-1) \sinh\left(\frac{1}{n+m+2\lambda-1}\right) \right]^{\frac{1}{2}(n+m-1)+\lambda} \\ &\sim \tilde{h}_m^\lambda n^{\frac{1}{2}(5m-n)} \sinh^{\frac{m-n}{2}} \left(\frac{1}{n-m}\right), \end{aligned} \quad (\text{B.2})$$

where  $\tilde{h}_m^\lambda = e^{5m/2} h_m^\lambda$ , and  $h_m^\lambda$  is a constant dependent on the parameters  $m$  and  $\lambda$ . Since  $1/(n-m)$  is small  $\forall_r n$ , we have

$$\sinh^{\frac{m-n}{2}} \left(\frac{1}{n-m}\right) \approx \left(\frac{1}{n-m}\right)^{\frac{m-n}{2}} \sim n^{-\frac{m-n}{2}} \quad \forall n \gg m. \quad (\text{B.3})$$

Substituting (B.3) into (B.2) yields

$$\hat{\chi}_{n,m}^\lambda \gtrsim \tilde{h}_m^\lambda n^{2m},$$

from which the proof is accomplished. □

## References

- [1] F. Mainardi, Fractional calculus and waves in linear viscoelasticity: An introduction to mathematical models, World Scientific, 2022.
- [2] R. Gorenflo, F. Mainardi, Random walk models for space-fractional diffusion processes, *Fract. Calc. Appl. Anal* 1 (1998) 167–191.
- [3] C. A. Monje, Y. Chen, B. M. Vinagre, D. Xue, V. Feliu-Batlle, Fractional-order systems and controls: fundamentals and applications, Springer Science & Business Media, 2010.

- [4] J. Zhang, F. Zhou, N. Mao, Numerical optimization algorithm for solving time-fractional telegraph equations, *Physica Scripta* 100 (2025).
- [5] A. Ghasempour, Y. Ordokhani, S. Sabermahani, Mittag-Leffler wavelets and their applications for solving fractional optimal control problems, *JVC/Journal of Vibration and Control* 31 (2025) 753 – 767.
- [6] K. Rabiei, M. Razzaghi, Fractional-order Boubaker wavelets method for solving fractional Riccati differential equations, *Applied Numerical Mathematics* 168 (2021) 221 – 234.
- [7] P. Rahimkhani, M. H. Heydari, Numerical investigation of  $\psi$ -fractional differential equations using wavelets neural networks, *Computational and Applied Mathematics* 44 (2025) 54.
- [8] D. Damircheli, M. Razzaghi, A wavelet collocation method for fractional Black–Scholes equations by subdiffusive model, *Numerical Methods for Partial Differential Equations* 40 (2024) e23103.
- [9] P. Rahimkhani, Y. Ordokhani, E. Babolian, Numerical solution of fractional pantograph differential equations by using generalized fractional-order Bernoulli wavelet, *Journal of Computational and Applied Mathematics* 309 (2017) 493–510.
- [10] Z. Barary, A. Y. Cherati, S. Nemati, An efficient numerical scheme for solving a general class of fractional differential equations via fractional-order hybrid Jacobi functions, *Communications in Nonlinear Science and Numerical Simulation* 128 (2024) 107599.
- [11] S. Deniz, F. Özger, Z. Ö. Özger, S. Mohiuddine, M. T. Ersoy, Numerical solution of fractional volterra integral equations based on rational Chebyshev approximation, *Miskolc Mathematical Notes* 24 (2023) 1287–1305.
- [12] O. Postavaru, An efficient numerical method based on Fibonacci polynomials to solve fractional differential equations, *Mathematics and Computers in Simulation* 212 (2023) 406–422.
- [13] S. Akhlaghi, M. Tavassoli Kajani, M. Allame, Application of Müntz orthogonal functions on the solution of the fractional Bagley–Torvik equation using collocation method with error estimate, *Advances in Mathematical Physics* 2023 (2023) 5520787.
- [14] H. Bazgir, B. Ghazanfari, Existence and uniqueness of solutions for fractional integro-differential equations and their numerical solutions, *International Journal of Applied and Computational Mathematics* 6 (2020) 122.
- [15] Y. Cao, M. A. Zaky, A. S. Hendy, W. Qiu, Optimal error analysis of space–time second-order difference scheme for semi-linear non-local Sobolev-type equations with weakly singular kernel, *Journal of Computational and Applied Mathematics* 431 (2023) 115287.
- [16] W. Qiu, D. Xu, J. Guo, The Crank-Nicolson-type Sinc-Galerkin method for the fourth-order partial integro-differential equation with a weakly singular kernel, *Applied Numerical Mathematics* 159 (2021) 239–258.
- [17] M. Cui, An alternating direction implicit compact finite difference scheme for the multi-term time-fractional mixed diffusion and diffusion–wave equation, *Mathematics and Computers in Simulation* 213 (2023) 194–210.
- [18] K. Diethelm, N. J. Ford, A. D. Freed, Y. Luchko, Algorithms for the fractional calculus: A selection of numerical methods, *Computer methods in applied mechanics and engineering* 194 (2005) 743–773.
- [19] Y. Edrisi-Tabriz, Using the integral operational matrix of B-spline functions to solve fractional optimal control problems, *Control and Optimization in Applied Mathematics* 7 (2022) 77–98.
- [20] I. Avcı, N. I. Mahmudov, Numerical solutions for multi-term fractional order differential equations with fractional Taylor operational matrix of fractional integration, *Mathematics* 8 (2020) 96.
- [21] Z. Xiaogang, N. Yufeng, An operational matrix method for fractional advection-diffusion equations with variable coefficients, *Applied Mathematics and Mechanics* 39 (2018) 104–112.
- [22] V. S. Krishnasamy, S. Mashayekhi, M. Razzaghi, Numerical solutions of fractional differential equations by using fractional Taylor basis, *IEEE/CAA Journal of Automatica Sinica* 4 (2017) 98–106.
- [23] O. Nikan, Z. Avazzadeh, Numerical simulation of fractional evolution model arising in viscoelastic mechanics, *Applied Numerical Mathematics* 169 (2021) 303–320.
- [24] S. Zhai, X. Feng, Investigations on several compact ADI methods for the 2D time fractional diffusion equation, *Numerical Heat Transfer, Part B: Fundamentals* 69 (2016) 364–376.
- [25] N. Thakoor, D. K. Behera, A new computational technique based on localized radial basis functions for fractal subdiffusion, in: *AIP Conference Proceedings*, volume 2768, AIP Publishing.
- [26] Y. Dimitrov, Approximations of the fractional integral and numerical solutions of fractional integral equations, *Communications on Applied Mathematics and Computation* 3 (2021) 545–569.
- [27] M. Ciesielski, G. Grodzki, Numerical approximations of the Riemann–Liouville and Riesz fractional integrals, *Informatica* 35 (2024) 21–46.
- [28] K. T. Elgindy, High-order numerical solution of second-order one-dimensional hyperbolic telegraph equation using a shifted Gegenbauer pseudospectral method, *Numerical Methods for Partial Differential Equations* 32 (2016) 307–349.
- [29] K. T. Elgindy, High-order, stable, and efficient pseudospectral method using barycentric Gegenbauer quadratures, *Applied Numerical Mathematics* 113 (2017) 1–25.
- [30] K. T. Elgindy, Optimal control of a parabolic distributed parameter system using a fully exponentially convergent barycentric shifted Gegenbauer integral pseudospectral method, *Journal of Industrial & Management Optimization* 14 (2018) 473.
- [31] K. T. Elgindy, H. M. Refat, High-order shifted Gegenbauer integral pseudo-spectral method for solving differential equations of Lane–Emden type, *Applied Numerical Mathematics* 128 (2018) 98–124.
- [32] K. T. Elgindy, The numerical approximation of Caputo fractional derivative of higher orders using a shifted Gegenbauer pseudospectral method: Two-point boundary value problems of the Bagley Torvik type case study, 2025.
- [33] K. T. Elgindy, H. M. Refat, Direct integral pseudospectral and integral spectral methods for solving a class of infinite horizon optimal output feedback control problems using rational and exponential Gegenbauer polynomials, *Mathematics and Computers in Simulation* 219 (2024) 297–320.
- [34] I. M. Batiha, S. Alshorm, A. Al-Husban, R. Saadeh, G. Gharib, S. Momani, The n-point composite fractional formula for approximating Riemann–Liouville integrator, *Symmetry* 15 (2023) 938.
- [35] K. T. Elgindy, K. A. Smith-Miles, Solving boundary value problems, integral, and integro-differential equations using Gegenbauer integration matrices, *Journal of Computational and Applied Mathematics* 237 (2013) 307–325.

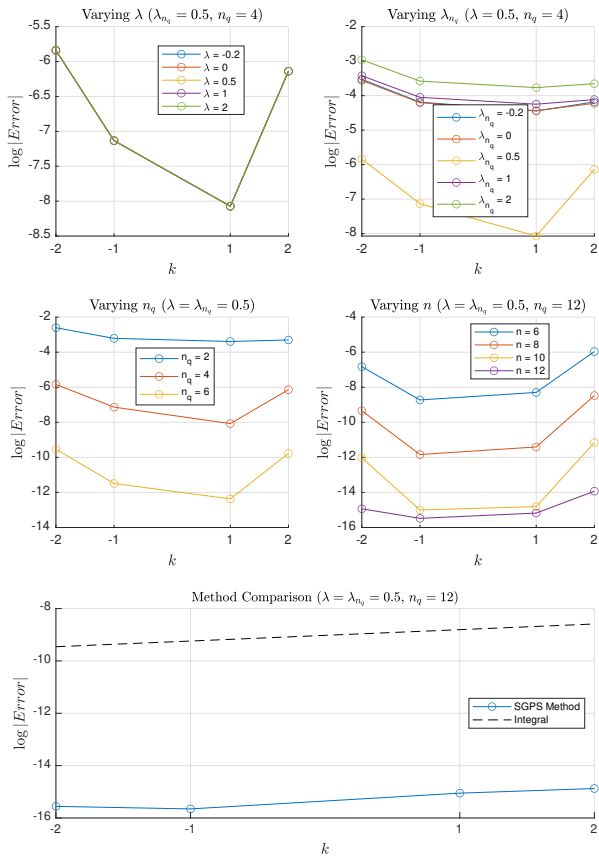


**Figure 4:** Logarithmic absolute errors of the RLFI approximations for the exponential function  $g$ , computed using the SGPS method. The fractional order is set to  $\alpha = 0.5$ , and the approximations are evaluated at  $t = 0.5$  using a 13th-degree Gegenbauer interpolant for  $k = -2, -1, 1, 2$ , except for the middle right subplot, where  $n$  varies. The figure presents errors under different conditions: *Top-left:* Varying  $\lambda$  with fixed  $\lambda_{n_q} = 0.5$  and  $n_q = 4$ . *Top-right:* Varying  $\lambda_{n_q}$  with fixed  $\lambda = 0.5$  and  $n_q = 4$ . *Middle-left:* Varying  $n_q$  with  $\lambda = \lambda_{n_q} = 0.5$ . *Middle-right:* Varying  $n$  with  $\lambda = \lambda_{n_q} = 0.5$  and  $n_q = 12$ . *Bottom:* Comparison between RLIM and MATLAB's `integral` function using  $n_q = 12$  and  $\lambda_1 = \lambda_2 = 0.5$ . "Error" refers to the difference between the true RLFI value and its approximation.

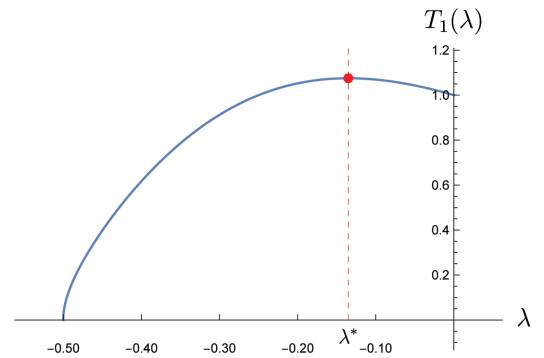


**Figure B.6:** Behavior of  $T_1$  for  $\lambda \in \mathbb{R}_{-1/2}^-$ . The red dashed line indicates  $\lambda = \lambda^* \approx -0.1351$ .

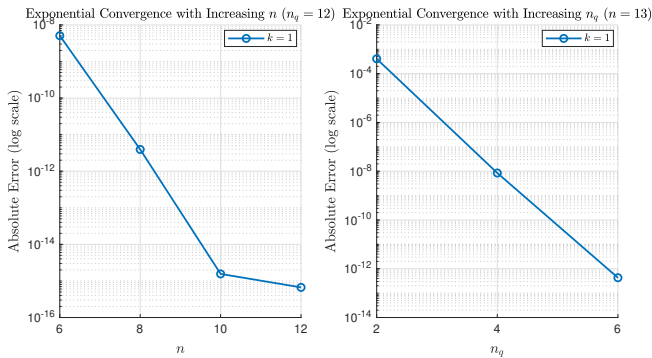


**Figure 5:** The left subplot demonstrates the exponential convergence of the absolute error as  $n$  increases, with  $n_q$  fixed at 12. The right subplot illustrates the exponential convergence of the absolute error as the  $n_q$  parameter increases, with  $n$  fixed at 13. Both subplots show the absolute error on a logarithmic scale.